Preparation, patterning and luminescent properties of oxyapatite $La_{9.33}(SiO_6)_4O_2$:A(A = Eu^{3+}, Tb^{3+}, Ce^{3+}) phosphor films by sol–gel soft lithography

2003 J. Phys.: Condens. Matter 15 2115

(http://iopscience.iop.org/0953-8984/15/12/328)

INSTITUTE OF PHYSICS PUBLISHING JOURNAL OF PHYSICS: CONDENSED MATTER

J. Phys.: Condens. Matter **15** (2003) 2115–2126 PII: S0953-8984(03)57451-3

Preparation, patterning and luminescent properties of oxyapatite $La_{9.33}(SiO_6)_4O_2$:A (A = Eu^{3+}, Tb^{3+}, Ce^{3+}) phosphor films by sol–gel soft lithography

X M Han[1], J Lin[1,3], R B Xing[2], J Fu[2], S B Wang[1] and Y C Han[2,3]

[1] Key Laboratory of Rare Earth Chemistry and Physics, Changchun Institute of Applied Chemistry, Chinese Academy of Sciences, Changchun 130022, People's Republic of China
[2] State Key Laboratory of Polymer Physics and Chemistry, Changchun Institute of Applied Chemistry Chinese Academy of Sciences, Changchun 130022, People's Republic of China

E-mail: jlin@ns.ciac.jl.cn

Received 13 December 2002
Published 17 March 2003
Online at stacks.iop.org/JPhysCM/15/2115

Abstract

Silicate oxyapatite $La_{9.33}(SiO_6)_4O_2$:A (A = Eu^{3+}, Tb^{3+} and/or Ce^{3+}) phosphor films and their patterning were fabricated by a sol–gel process combined with soft lithography. X-ray diffraction (XRD), Fourier transform infrared spectroscopy, atomic force microscopy, optical microscopy and photoluminescence spectra, as well as lifetimes, were used to characterize the resulting films. The results of XRD indicated that the films began to crystallize at 800 °C and the crystallinity increased with the increase in annealing temperatures. Transparent nonpatterned phosphor films were uniform and crack-free, which mainly consisted of rodlike grains with a size between 150 and 210 nm. Patterned thin films with different bandwidths (20, 50 μm) were obtained by the micromoulding in capillaries technique. The doped rare earth ions (Eu^{3+}, Tb^{3+} and Ce^{3+}) showed their characteristic emission in crystalline $La_{9.33}(SiO_6)_4O_2$ phosphor films, i.e. Eu^{3+} $^5D_0$–^7F_J ($J = 0, 1, 2, 3, 4$), Tb^{3+} $^5D_{3,4}$–^7F_J ($J = 3, 4, 5, 6$) and Ce^{3+} 5d(^{2}D)–4f($^2F_{2/5}$, $^2F_{2/7}$) emissions, respectively. Both the lifetimes and PL intensity of the Eu^{3+}, Tb^{3+} ions increased with increasing annealing temperature from 800 to 1100 °C, and the optimum concentrations for Eu^{3+}, Tb^{3+} were determined to be 9 and 7 mol% of La^{3+} in $La_{9.33}(SiO_6)_4O_2$ films, respectively. An energy transfer from Ce^{3+} to Tb^{3+} was observed in the $La_{9.33}(SiO_6)_4O_2$:Ce, Tb phosphor films, and the energy transfer efficiency was estimated as a function of Tb^{3+} concentration.

[3] Authors to whom any correspondence should be addressed.

1. Introduction

Phosphors are applied to faceplates either in powder form or in thin film form. In the first case, the powder phosphors are mixed with organic binders to spread on a substrate, while in the latter case thin film phosphors are deposited on a substrate followed by subsequent annealing. In 1980, Robertson [1] found that rare earth-doped garnet luminescent films epitaxially grown on single-crystal substrates could withstand much higher power densities than with powder phosphors without tube degradation. Since then thin film phosphors have been attracting much attention [2–7]. In thin film phosphors, the uniform thickness combined with smoother surface morphology and smaller grain size makes it possible to define a smaller pixel spot size and thus achieve a higher resolution.

Our group [8–10] and others [11–13] have been focusing on the preparation of luminescent films via the sol–gel route, which possesses a number of advantages over conventional film formation techniques, such as low processing temperature, easy coating of large surfaces, possible formation of porous films and homogeneous multicomponent oxide films, and simple and cheap experimental set-ups [14]. $La_{9.33}(SiO_4)_6O_2$ belongs to the rare-earth–metal silicates with an oxyapatite structure, which have been used as host materials for the luminescence of various rare earth and mercury-like ions [15–17]. The most prominent structural characteristic is the two rare-earth sites in the oxyapatite host lattice, i.e. the nine-coordinate 4f site with C_3 point symmetry and the seven-coordinate 6h site with C_S point symmetry. Both sites are very suitable for the luminescence of rare earth ions (4f–4f and 5d–4f emissions) due to their low symmetry features [15–17]. So far, no phosphor film based on a $La_{9.33}(SiO_4)_6O_2$ host has been reported. Therefore, we report a sol–gel synthesis of nanocrystalline $La_{9.33}(SiO_4)_6O_2$:A (A = Eu^{3+}, Tb^{3+}, Ce^{3+}) thin phosphor films in this paper. Furthermore, the patterning of the film via soft lithography (micromoulding in capillaries) and their photoluminescence (PL) properties are also reported in this context.

2. Experimental section

Non-patterned thin films of $La_{9.33}(SiO_4)_6O_2$:A (A = Eu^{3+}, Tb^{3+} and/or Ce^{3+}) phosphor samples were prepared by a sol–gel and dip-coating method [9]. The doping concentration of the rare earth ion (A) was 1–15 mol% that of La^{3+} in the $La_{9.33}(SiO_4)_6O_2$ host. Stoichiometric amounts of La_2O_3 (99.9%), Eu_2O_3 (99.99%), Tb_4O_7 (99.9%) and $Ce(NO_3)_3{\cdot}6H_2O$ (99.99%) were dissolved in concentrated HNO_3 (A.R.), and were then mixed with a water–ethanol (v/v = 1:4) solution. Then a stoichiometric amount of $Si(OC_2H_5)_4$ (TEOS) was added. The solution was stirred for 2 h to form a sol and dip-coated on thoroughly cleaned silica glass substrates at a speed of 0.2 cm s^{-1}. The coatings were dried at 100 °C for 1 h immediately. Then the dried films were annealed to the desired temperature (700–1200 °C) with a heating rate of 1 °C min^{-1} and held there for 2 h in air (for A = Eu^{3+}) or in a mixed atmosphere of 95% nitrogen and 5% hydrogen (for A = Tb^{3+} and/or Ce^{3+}).

The patterning of the phosphor films was carried out by soft lithography as described previously [18]. The polydimethylsiloxane (PDMS) stamp modes (with different channel widths of 20 and 50 μm) were placed in conformal contact with thoroughly cleaned silicon wafer substrates. The channels of the mode thus formed capillaries with the silicon wafer substrate. The above sol for dip-coating was then dropped at the open end with a transfer pipette. The capillary force made the sol flow into the mould. Then the modes and substrates were dried at 100 °C overnight. After carefully removing the modes, the resulted patterned gel films were heated to 500 °C with a heating rate of 1 °C min^{-1} and held there for 2 h in air. The preheated film samples were fired at the rate of 100 °C h^{-1} to the desired temperature (700–1200 °C) for 2 h.

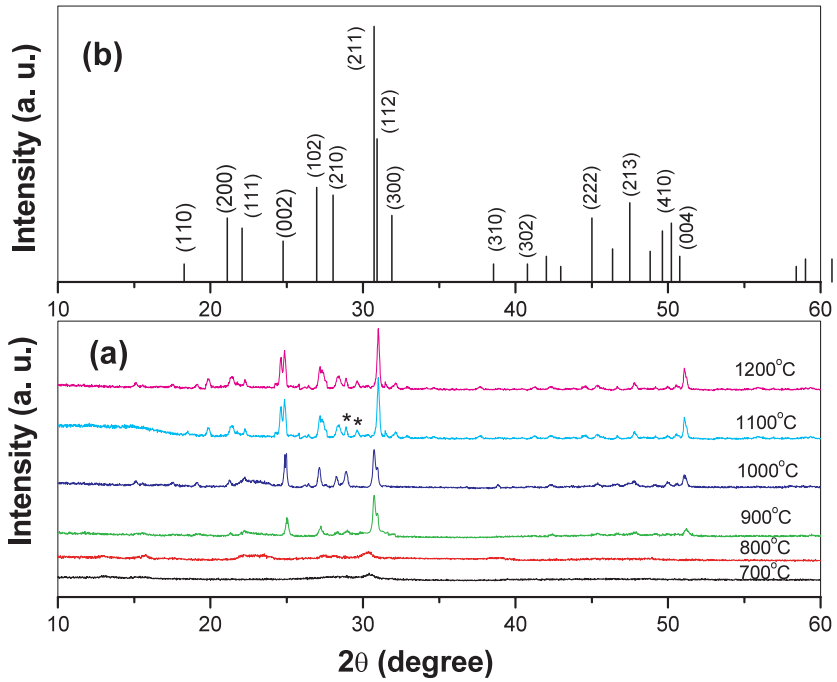

Figure 1. XRD patterns for $La_{8.49}Eu_{0.84}(SiO_4)_6O_2$ films annealed at different temperatures (a) and standard JCPDS Card 49-0443 for $La_{9.33}(SiO_4)_6O_2$ (b).

The x-ray diffraction (XRD) of the film and powder samples was examined on a Rigaku–Dmax 2500 diffractometer using Cu Kα radiation ($\lambda = 0.154\,05$ nm). FT-IR spectra were measured with a Perkin-Elmer 580B infrared spectrophotometer with the KBr pellet technique. A TA Instruments thermal analyser was used to record TGA–DTA curves of the gel powders with a heating rate of 10 °C min^{-1}. The morphology of the crystalline film sample was inspected using atomic force microscope (AFM, Seiko) with a taping mode. Patterned film pictures were taken on a Lcica DMLP optical microscope. The excitation and emission spectra were taken on a Hitachi F-4500 spectrofluorimeter equipped with a 150 W xenon lamp as the excitation source. Luminescence lifetimes were measured with a SPEX 1934D phosphorimeter using a 7 W pulse xenon lamp as the excitation source with a pulse width of 3 μs. All the measurements were performed at room temperature (RT).

3. Results and discussion

3.1. Formation and morphology of the phosphor films.

XRD. Figure 1(a) shows XRD patterns of film samples annealed at different temperatures from 700 to 1200 °C at intervals of 100 °C. For films annealed at 700 °C, no diffraction peaks are observed. This indicates that the film remains amorphous below this temperature. For the sample fired at 800 °C, a weak and broad peak at $2\theta = 30.92°$ is present in the XRD pattern, which is assigned to the (211) reflection of oxyapatite $La_{9.33}(SiO_4)_6O_2$, suggesting the starting of crystallization at this stage. At 900 °C, other diffraction peaks at $2\theta = 24.97°, 27.17°, 51.20°$ belonging to crystalline oxyapatite are observed according to the standard card (JCPDS Card 49-0443 in figure 1(b)). These diffraction peaks increase

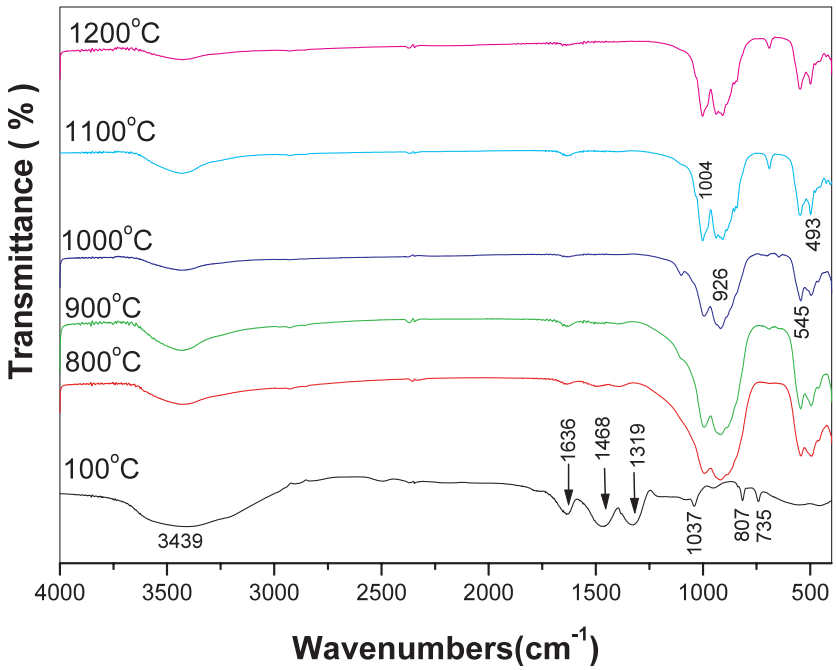

Figure 2. FT-IR spectra of $La_{8.49}Eu_{0.84}(SiO_4)_6O_2$ powders annealed at different temperatures.

in intensity with further increase of the annealing temperature, and no difference in width and intensity is observed for the 1100 and 1200 °C sintered samples, indicating that the crystallization of $La_{9.33}(SiO_4)_6O_2$ is complete at 1100 °C. This temperature is about 200 °C lower than that of the powder $La_{9.33}(SiO_4)_6O_2$ [17]. Also note that two peaks at $2\theta = 28.86°$, 29.65 ° not belonging to crystalline $La_{9.33}(SiO_4)_6O_2$ appeared in 1100 and 1200 °C annealed samples, which belong to $La_2Si_2O_7$ due to the reaction of La_2O_3 with the silica substrates.

FT-IR. FT-IR spectra were recorded using the gel powders annealed at various temperatures, as shown on figure 2. For the sample after heat treatment at 100 °C, the FT-IR spectrum shows three main absorption regions. The first (a broad band) in the range 2750–3750 cm^{-1}, with a maximum at 3439 cm^{-1}, arises from the absorption of O–H groups; the second region in the range 1250–1750 cm^{-1} originates from the absorption of H_2O (1636 cm^{-1}) and NO_{3^-} groups (1468, 1319 cm^{-1}), respectively; and the third region with peak at 1037 cm^{-1}originates from the adsorption of Si–O–Si asymmetric stretching vibrations. Significant changes are observed with further heat treatment. After heating at 800 °C, the absorption peaks from −OH, H_2O and NO_{3^-} become weak, and a new broad absorption band peaking at 926 cm^{-1} is present, which arises from the asymmetric stretching vibration of SiO_4 groups. A new absorption peak at 545 cm^{-1} due to a bending vibration of O–Si–O bonds is present, and the absorption bands of SiO_4 groups remain broad, implying the amorphous character of the samples. Heat treatment between 900 to 1200 °C leads the absorption peaks of SiO_4 to be more structured, suggesting that crystallized silicate oxyapatite has formed.

AFM and optical micrographs. The morphology of the crystalline film sample was inspected using an AFM. The AFM image of the transparent film annealed at 1100 °C is shown in figure 3. It is known from planar images that the film, which is uniform and crack-free, mainly consists

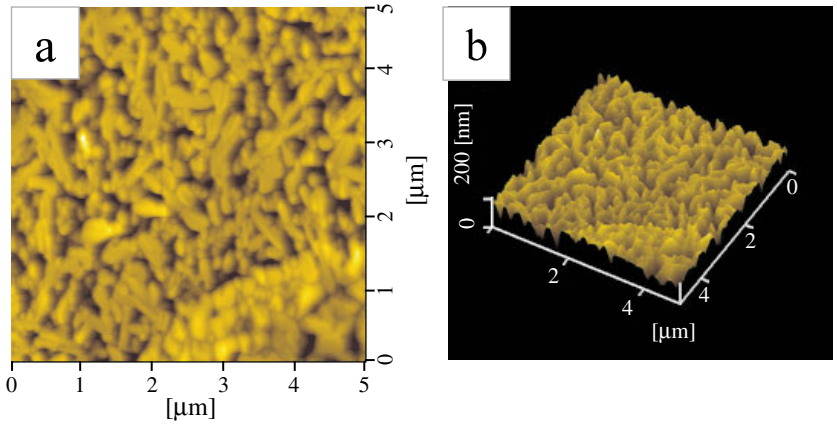

Figure 3. AFM images of the $La_{8.49}Eu_{0.84}(SiO_4)_6O_2$ film annealed at 1100 °C: (a) planar image, (b) stereo image.

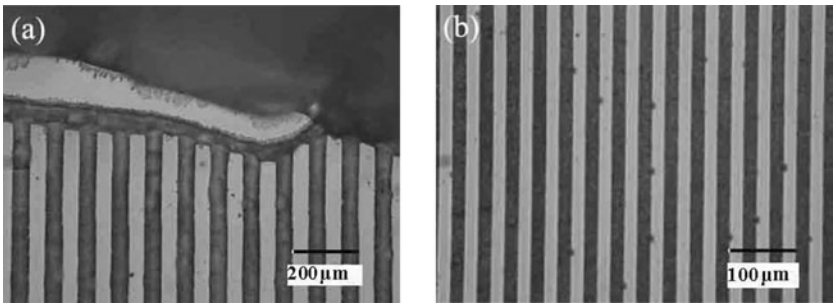

Figure 4. Optical micrographs of the patterned $La_{8.49}Eu_{0.84}(SiO_4)_6O_2$ gel films with a linewidth of 50 μm (a) and 20 μm (b).

of closely packed rodlike particles with an average between 150 and 210 nm (figure 3(a)). The film surface is well crystallized with a roughness (RMS) of 58.7 nm (stereo image in figure 3(b)).

The patterning of the phosphor films was performed in a Eu^{3+}-doped $La_{9.33}(SiO_4)_6O_2$ system. Figures 4(a), (b) show optical micrographs for the patterned structures of $La_{9.33}Eu_{0.84}(SiO_4)_6O_{24}$ gel (100 °C dried) films with linewidths of 50 and 20 μm, respectively. The dark and bright regions correspond to the film's bands and spaces, respectively. Defect-free gel film bands having widths of 50 μm (spaced by 50 μm) and 20 μm (spaced by 20 μm) can be seen clearly in figures 4(a) and (b), respectively. From figure 4(a) one can observe clearly how the film bands were produced. At the open end the sol flowed into the channels between the substrate and the mode, forming patterned gel film stripes after drying. A layer of nonpatterned film, formed from the left sol that did not flow into the channel, can be seen clearly. We noted that, after firing, a significant shrinkage (nearly 50%) was observed for the film bands due to solvent evaporation and crystallization. The patterning technologies of phosphor screens have a great effect on the resolution of flat panel display devices [19]. For instance, pitches of phosphor lines for a supervideo graphics adapter with 800 × 600 lines, video graphics adapter with 640 × 480 lines and quarter video graphics adapter with 320 × 240 lines in 6 inch colour displays are defined as 50.8, 63.5 and 127 μm, respectively. The current

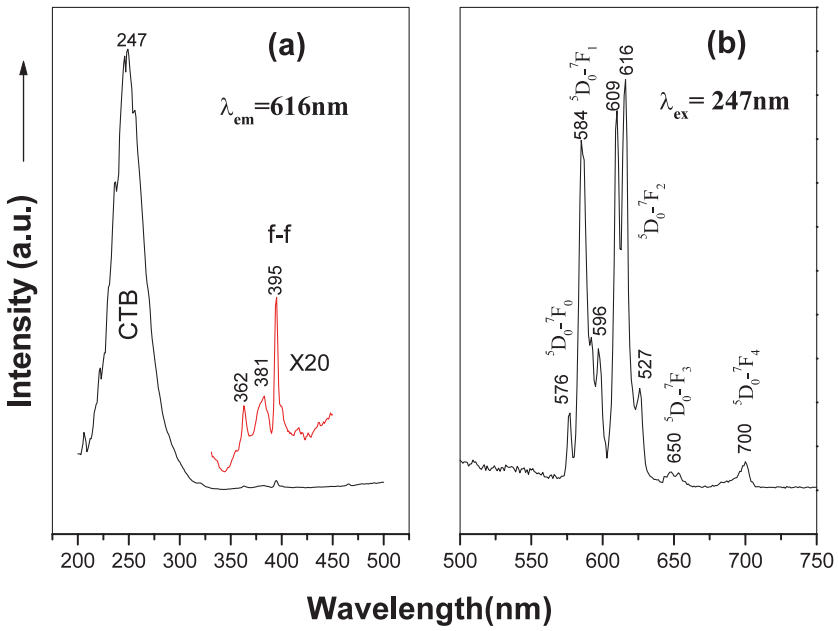

Figure 5. Excitation (a) and emission (b) spectra for $La_{8.49}Eu_{0.84}(SiO_4)_6O_2$ film.

patterning techniques used for phosphor screens include electrophoretic deposition [20] and screen printing [21], etc, based on photolithography, which need complicated and expensive photolithographic and etching equipment. Here we provide a simple process to prepare the patterned phosphor films, which are promising for future applications in the display fields.

3.2. Photoluminescence properties

$La_{9.33}(SiO_4)_6O_2:Eu^{3+}$ films. Eu^{3+}-doped $La_{9.33}(SiO_4)_6O_2$ thin films display a bright red emission under the excitation of UV light. Figure 5 shows the excitation and emission spectrum for a $La_{8.49}Eu_{0.84}(SiO_4)_6O_2$ film annealed at 1100 °C. The excitation spectrum (figure 5(a)) consists of a broad intense band with a maximum at 247 nm and some weak lines between 300 and 500 nm. The former is due to the charge transfer band (CTB) of Eu^{3+}–O^{2-}, and the latter is from f–f transitions within the Eu^{3+} $4f^6$ electron configuration. Upon excitation into the CTB at 247 nm, the obtained emission spectrum (figure 5(b)) is composed of $^5D_0$–^7F_J ($J = 1, 2, 3, 4$) emission lines of Eu^{3+}, with the hypersensitive red emission transition $^5D_0$–$^7F_2$ (616 nm) being the most prominent group, agreeing well with the low local symmetry (C_3 and/or Cs) for Eu^{3+} in the host lattice [9, 15, 16].

The PL decay curve of Eu^{3+} in $La_{9.33}(SiO_4)_6O_2$ films sintered at 1100 °C is shown in figure 6. This curve can be well fitted into a single exponential function as $I = I_0 \exp[-t/\tau]$ (I_0 is the initial intensity at $t = 0$ and τ is the $1/e$ lifetime), from which the lifetimes of Eu^{3+} are determined. The PL intensity and lifetimes for Eu^{3+} in $La_{8.49}Eu_{0.84}(SiO_4)_6O_2$ films have been investigated as a function of annealing temperatures from 700 to 1200 °C. It is found that both the PL intensity and the lifetimes of Eu^{3+} increase with the annealing temperature in the films, as shown in figure 7. This is due to the fact that the content of impurities in the film, such as −OH, OR, H_2O, NO_3^-, etc, decreases with increase in annealing temperature. The quenching of the luminescence of Eu^{3+} by excitation of the vibrations of these impurities decreases,

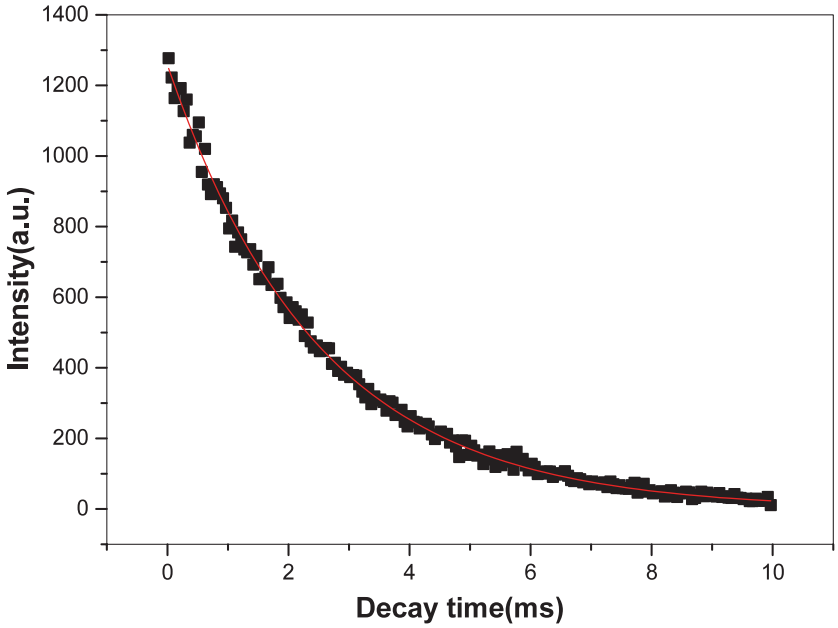

Figure 6. The decay curves of Eu^{3+} ($^5D_0$–$^7F_2$) luminescence in a crystalline $La_{8.49}Eu_{0.84}(SiO_4)_6O_2$ film annealed at 1100 °C.

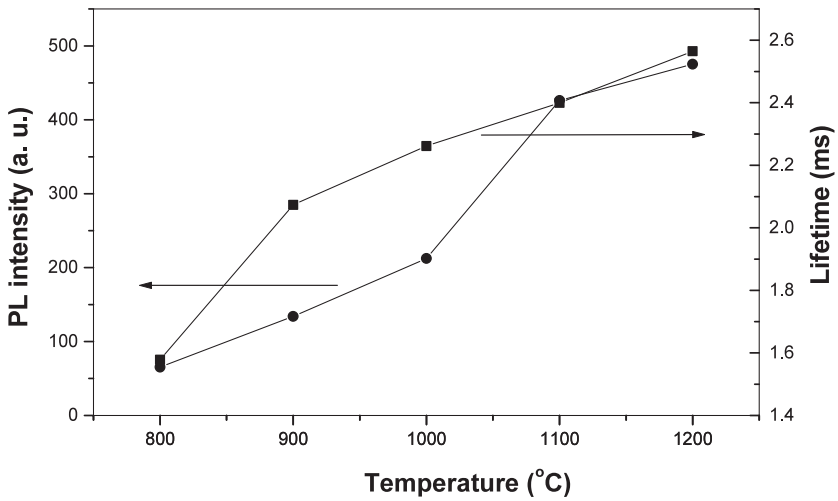

Figure 7. The emission intensity and lifetimes of Eu^{3+} as a function of annealing temperature in a $La_{8.49}Eu_{0.84}(SiO_4)_6O_2$ film.

resulting in the increase of PL intensity and lifetimes of Eu^{3+}. In addition, the PL intensity and lifetimes of Eu^{3+} have also been studied as a function of Eu^{3+} doping concentration (x) in $La_{9.33(1-x)}Eu_{9.33x}(SiO_4)_6O_2$ films, as shown in figure 8. Both the PL intensity and lifetimes of Eu^{3+} first increase with Eu^{3+} concentration, reaching a maximum at $x = 0.09$, and then decrease with further increase in concentration (x) due to the concentration quenching effect. Thus the optimum concentration of Eu^{3+} is 9 mol% that of La^{3+} in the $La_{9.33}(SiO_4)_6O_2$ film.

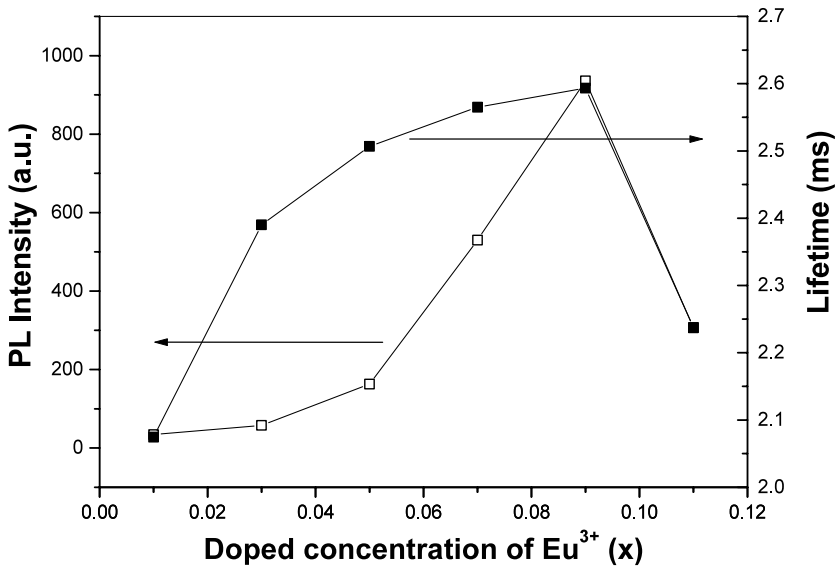

Figure 8. The emission intensity and lifetimes of Eu^{3+} as a function of its doping concentration (x) in $La_{9.33(1-x)}Eu_{9.33x}(SiO_4)_6O_2$ films annealed at 1100 °C.

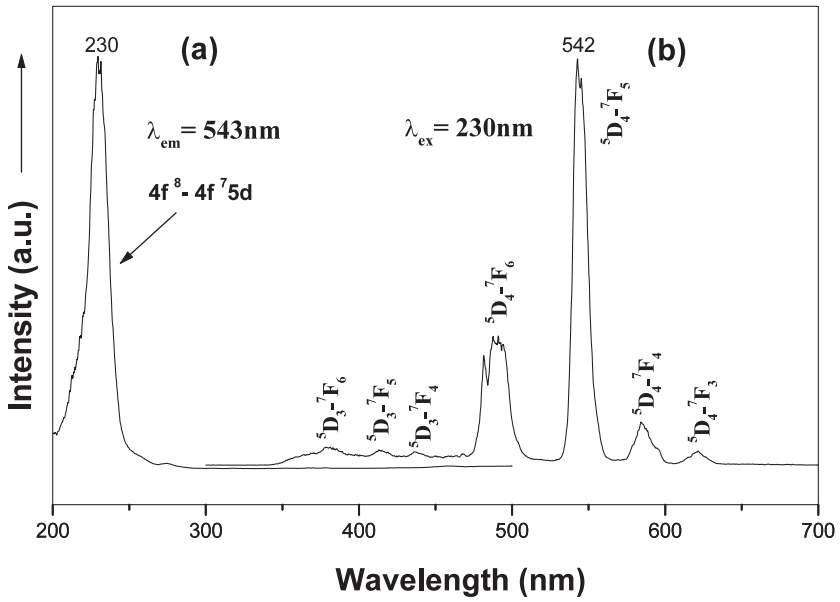

Figure 9. Excitation (a) and emission (b) spectra for a $La_{8.68}Tb_{0.65}(SiO_4)_6O_2$ film annealed at 1100 °C.

$La_{9.33}(Si\,O_4)_6\,O_2$:Tb films. Tb^{3+}-doped $La_{9.33}(SiO_4)_6O_2$ films show a blue or green emission, depending on its doping concentrations. Figures 9(a) and (b) show the excitation and emission spectra of $La_{8.68}Tb_{0.65}$ $(SiO_4)_6O_2$ thin film, respectively. The excitation spectrum (figure 9(a)) of Tb^{3+} contains an intense broad band with a maximum at 230 nm due to the spin-allowed $4f^8$–$4f^7$5d transition. The forbidden f–f excitation transitions of Tb^{3+} cannot be observed

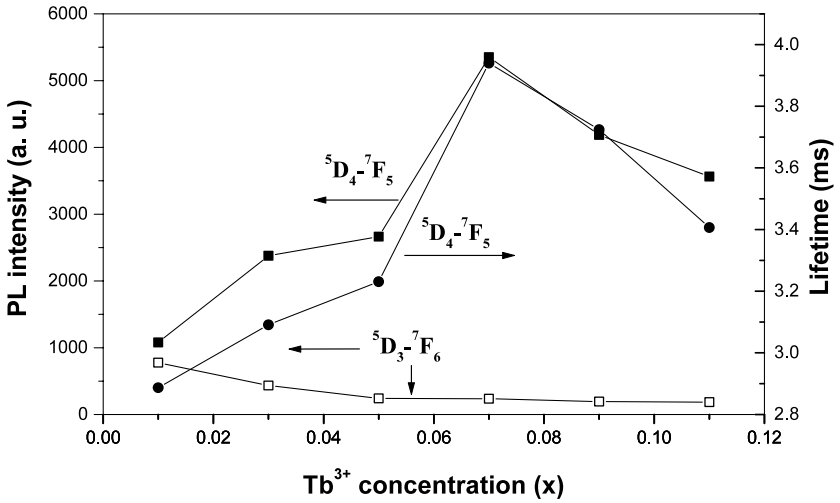

Figure 10. The emission intensity of Tb^{3+} ($^5D_4$–$^7F_5$), ($^5D_3$–$^7F_6$) and lifetimes ($^5D_4$) as a function of its concentration (x) in crystalline $La_{9.33(1-x)}Tb_{9.33x}(SiO_4)_6O_2$ films annealed at 1100 °C.

clearly due to their weak intensity relative to the allowed $4f^8$–$4f^75d$ transition. However, these f–f excitation lines can be seen clearly if the spectrum is displayed at a higher magnification. Excitation into the $4f^8$–$4f^75d$ band at 230 nm yields the characteristic blue and green emission lines of Tb^{3+} $^5D_{3,4}$–^7F_J ($J = 3, 4, 5, 6$) transitions, with the $^5D_4$–$^7F_5$ (543 nm) green emission as the most prominent feature (figure 9(b)). Figure 10 shows the concentration dependence of the Tb^{3+} $^5D_3$–$^7F_6$ and $^5D_4$–$^7F_5$ emission intensities in $La_{9.33(1-x)}Tb_{9.33x}(SiO_4)_6O_2$ films. Note that, with the increase of Tb^{3+} concentration, the intensity of the latter increases gradually until $x = 0.07$ at the cost of the intensity of the former. This is due to the cross-relaxation effect between $^5D_3$–$^5D_4$ and $^7F_0$–$^7F_6$ of Tb^{3+} [16]. The decrease of the emission intensity of $^5D_4$–$^7F_5$ after $x = 0.07$ is due to the concentration quenching effect. This is also in agreement with the concentration dependence of the lifetimes of Tb^{3+} ($^5D_4$), as shown in the same figure.

$La_{9.33}(SiO_4)_6O_2$:Ce and $La_{9.33}(SiO_4)_6O_2$:Ce, Tb films. The Ce^{3+} ion shows a UV-blue emission in the crystalline $La_{9.33}(SiO_4)_6O_2$ film. The excitation and emission spectra of a $La_{7.93}Ce_{1.40}(SiO_4)_6O_2$ film are shown in figure 11. Independent of the monitored emission wavelength (355 or 381 nm), the excitation spectra consist of four bands with maxima at 244, 289, 314 and 332 nm (figure 11(a)), corresponding to the transitions from the ground state $^2F_{5/2}$ of Ce^{3+} to the different components of the excited 5d states of Ce^{3+} split by the crystal field. Excitation into the Ce^{3+} bands at 289, 314 or 332 nm yields the emission spectra with a similar profile (figure 11(b)), which include a double band with maxima at 355 and 381 nm assigned to the parity-allowed transitions from the lowest component of ^2D state to the spin–orbit components of the ground state, $^2F_{5/2}$ and $^2F_{7/2}$ of Ce^{3+}, respectively. The energy difference between the two emission peaks is 1922 cm^{-1}, basically agreeing with the ground state splitting of Ce^{3+} (2000 cm^{-1}, i.e. energy difference between the $^2F_{5/2}$ and $^2F_{7/2}$ doublets in the $4f^1$ configuration of the Ce^{3+} ion). According to the present results, it seems that there is only one kind of luminescent centre for the Ce^{3+}, indicating that the Ce^{3+} ions mainly occupy one site (4f site or 6h site) in the host lattice. However, it is not excluded that a minor amount of Ce^{3+} ions occupy the second site because there is a tail in the longer wavelength region of the emission spectrum.

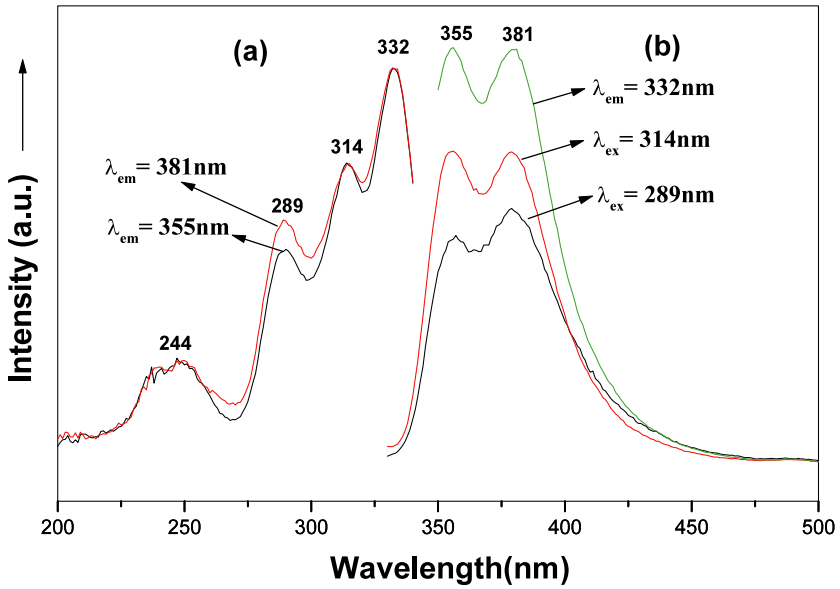

Figure 11. Excitation (a) and emission (b) spectra for a $La_{7.93}Ce_{1.40}(SiO_4)_6O_2$ film annealed at 1100 °C.

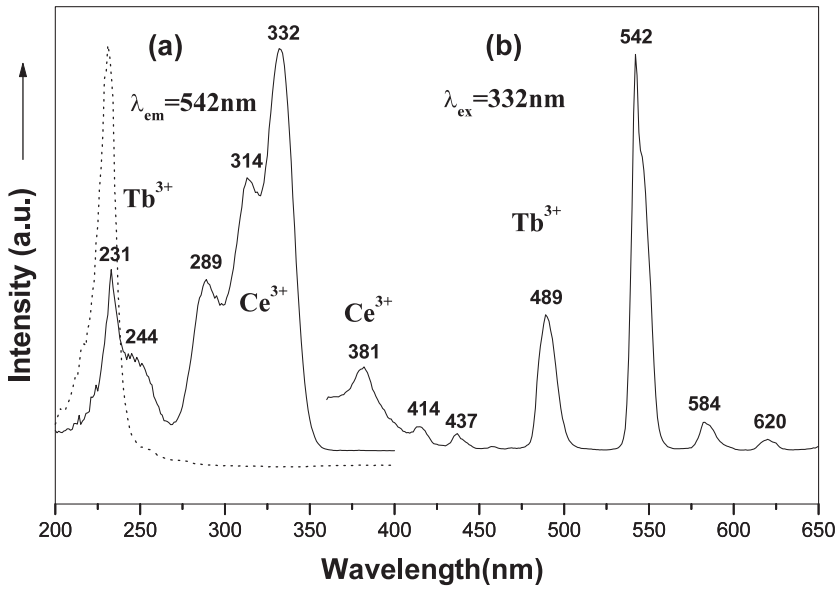

Figure 12. Excitation (a) and emission (b) spectra for a $La_{7.28}Ce_{1.40}Tb_{0.65}(SiO_4)_6O_2$ film annealed at 1100 °C. The dotted curve on the left shows the excitation spectrum of a $La_{8.68}Tb_{0.65}(SiO_4)_6O_2$ film as a comparison.

If the thin films of $La_{9.33}(SiO_4)_6O_2$ are codoped with cerium and terbium, they show a strong green luminescence under UV excitation caused by the line emission of Tb^{3+} ions. A typical excitation and emission spectrum for a film sample with composition $La_{7.28}Ce_{1.40}Tb_{0.65}(SiO_4)_6O_2$ is shown in figure 12. The excitation spectrum (figure 12(a))

Table 1. The integrated emission intensity of Ce^{3+}, Tb^{3+} and energy transfer efficiency (η_{ET}) from Ce^{3+} to Tb^{3+} in $La_{7.93(1-x)}Ce_{1.40}Tb_{7.93x}(SiO_4)_6O_2$ ($x = 0$–0.15) films (annealed at 1100 °C) upon excitation into the Ce^{3+} at 332 nm.

	x				
	0	0.01	0.05	0.10	0.15
I (Ce^{3+})	8467	7566	4849	1370	1094
I (Tb^{3+}, 542 nm)	0	1650	7590	4040	5330
η_{ET} (%)		10.6	42.7	83.8	87.1

monitored by the Tb^{3+} ($^5D_4$–$^7F_5$ at 542 nm) clearly shows two groups of bands at 231 nm (with a shoulder at 244 nm) and 288, 314, 332 nm, respectively. Comparing this excitation spectrum with those of $La_{9.33}(SiO_4)_6O_2$:Tb (figure 9(a)) and $La_{9.33}(SiO_4)_6O_2$:Ce (figure 11(a)), we can deduce that the first one (231 nm) is due to a $4f^8$–$4f^75d$ transition of Tb^{3+} and the latter (including the shoulder at 244 nm) is caused by Ce^{3+} 4f–5d transitions. The presence of the Ce^{3+} excitation bands in the excitation spectrum of Tb^{3+} (monitored by Tb^{3+} emission at 542 nm) suggests that an energy transfer occurs from Ce^{3+} to Tb^{3+} in a $La_{7.28}Ce_{1.40}Tb_{0.65}(SiO_4)_6O_2$ film. Upon excitation into the Ce^{3+} absorption band at 332 nm, the emission spectrum shows a very weak Ce^{3+} emission band around 381 nm and a group of strong Tb^{3+} $^5D_{3,4}$–^7F_J ($J = 3, 4, 5, 6$) emission bands with a green $^5D_4$–$^7F_5$ (542 nm) transition as the most prominent one, indicating an efficient energy transfer from Ce^{3+} to Tb^{3+}. The energy transfer from Ce^{3+} to Tb^{3+} is also well known in other host lattices [16], which can be ascribed to the spectral overlap between the 5d–4f band emission of Ce^{3+} and the 4f–4f excitation lines (enlarged part in figure 5(a)) of Tb^{3+} in the range of 300–500 nm.

The energy transfer efficiency from a donor (Ce^{3+}) to an acceptor (Tb^{3+}) can be calculated according to the formula $\eta_{ET} = 1 - I_d/I_{d0}$, where I_d and I_{d0} are the corresponding luminescence intensities of the donor (Ce^{3+}) in the presence and absence of the acceptor (Tb^{3+}) for the same donor (Ce^{3+}) concentration, respectively [22]. We investigated systematically the energy transfer efficiencies from Ce^{3+} to Tb^{3+} in $La_{7.93(1-x)}Ce_{1.40}Tb_{7.93x}(SiO_4)_6O_2$ ($x = 0$–0.15) film systems and the results are listed in table 1. Clearly, it is known from table 1 that, with the increase of Tb^{3+} concentration, the energy transfer efficiency from Ce^{3+} to Tb^{3+} increases gradually. This is because the energy transfer probability from Ce^{3+} to Tb^{3+} is proportional to R^{-6} (R is the average distance between Ce^{3+} and Tb^{3+}) [23]. However, with the increase of Tb^{3+} concentration (x) in $La_{7.93(1-x)}Ce_{1.40}Tb_{7.93x}(SiO_4)_6O_2$ ($x = 0$–0.15) film systems, there is a trend that the emission intensity of Tb^{3+} (542 nm) increases from $x = 0$ to 0.05 (maximum), then begins to decrease. This is due to the self-concentration quenching of Tb^{3+} luminescence. Furthermore, it is noted that the excitation intensity of the Tb^{3+} $4f^8$–$4f^75d$ transition at 231 nm in Ce^{3+}, Tb^{3+}-codoped phosphor films becomes much weaker in comparison with that in the corresponding Tb^{3+}-doped phosphor films (see figure 12), indicating that the excitation of Tb^{3+} in the former occurs mainly through the excitation of Ce^{3+}. Owing to the strong interaction between Ce^{3+} and Tb^{3+}, i.e. $Ce^{3+} \rightarrow Tb^{3+}$ energy transfer, the Tb^{3+} becomes more easily excited by Ce^{3+} than by Tb^{3+} itself [16]. This can be attributed to the competition of the UV excitation energy between Ce^{3+} and Tb^{3+} in the Ce^{3+}, Tb^{3+}-codoped phosphor films. As a result, when excited at 231 nm for a Tb^{3+} $4f^8$–$4f^75d$ transition, the emission intensity of Tb^{3+} (f–f transition at 542 nm) in Ce^{3+}, Tb^{3+}-codoped phosphor films is weaker than that in Tb^{3+}-doped phosphor films.

4. Conclusions

Silicate oxyapatite $La_{9.33}(SiO_6)_4O_2$:A (A = Eu^{3+}, Tb^{3+} and/or Ce^{3+}) phosphor films have been successfully fabricated by a sol–gel process, and these phosphor films can be patterned into ordered bands with different widths (20–50 μm) by a soft lithography technique (micromoulding in capillaries). The rare earth ions Eu^{3+}, Tb^{3+} and Ce^{3+} show strong emission with red (615 nm), green (542 nm) and blue (350–450 nm) colours, respectively, in the films. The optimum concentrations for the luminescence of Eu^{3+}, Tb^{3+} were determined to be 9 and 7 mol% of La^{3+} in $La_{9.33}(SiO_6)_4O_2$ films, respectively. There exists an energy transfer from Ce^{3+} to Tb^{3+} in a $La_{9.33}(SiO_6)_4O_2$:Ce, Tb film, in which the energy transfer efficiency depends on the concentration of Tb^{3+} in a fixed Ce^{3+} concentration.

Acknowledgments

This project is financially supported by the foundation of 'Bairen Jihua' of Chinese Academy of Sciences, the Outstanding Youth Fund of Jilin Province (20010103), National Natural Science Foundation of China for Distinguished Young Scholars (50225205, 50125311) and the Nanometer Center of Changchun Institute of Applied Chemistry, Chinese Academy of Sciences.

References

[1] Robertson J M and Tol M T van 1980 *Appl. Phys. Lett.* **37** 471
[2] Park S, Clark B L, Keszler D A, Bender J P, Wager J F, Reynolds T A and Herman G S 2002 *Science* **297** 65
[3] Frindell K L, Bartl M H, Popitsch A and Stucky G D 2002 *Angew. Chem., Int. Ed. Engl.* **41** 960
[4] Lee Y E, Norton D P, Budai J D, Rack P D and Potter M D 2000 *Appl. Phys. Lett.* **77** 678
[5] Jones S L, Kumar D, Singh R K and Holloway P H 1997 *Appl. Phys. Lett.* **71** 404
[6] Ouyang X, Kitai A H and Xiao T 1997 *J. Appl. Phys.* **71** 404
[7] Golego N, Studenikin S A and Cocivera M 2000 *J. Electrochem. Soc.* **147** 1993
[8] Lin J, Saenger D U, Mennig M and Baerner K 2000 *Thin Solid Films* **360** 39
[9] Yu M, Lin J, Zhou Y H, Wang S B and Zhang H J 2002 *J. Mater. Chem.* **12** 86
[10] Meng Q, Lin J, Fu L, Zhang H, Wang S and Zhou Y 2001 *J. Mater. Chem.* **11** 3382
[11] Rao R P 1996 *Solid State Commun.* **99** 439
[12] Choe J Y, Ravichandran D, Biomquist S M, Morton D C, Kirchner K W, Ervin M H and Lee U 2001 *Appl. Phys. Lett.* **78** 3800
[13] Ravichandran D, Roy R, Chakhovskoi A G, Hunt C E, White W B and Erdei S 1997 *J. Lumin.* **71** 291
[14] Sakka S 1996 *Struct. Bonding* **85** 1
[15] Lin J and Su Q 1994 *Mater. Chem. Phys.* **38** 98
[16] Lin J and Su Q 1995 *J. Mater. Chem.* **5** 1151
[17] Lammers M J J and Blasse G 1987 *J. Electrochem. Soc.* **134** 2068
[18] Seraji S, Wu Y, Jewell-Larson N E, Forbess M J, Limmer S J, Chou T P and Cao G 2000 *Adv. Mater.* **12** 1421
[19] Jang J E, Gwak J-H, Jin Y W, Lee S J, Park S H, Jung J E, Lee N S and Kim J M 2000 *J. Vac. Sci. Technol.* B **18** 1106
[20] Sluzky E and Hesse K 1989 *J. Electrochem. Soc.* **126** 2742
[21] Holmes P J and Loasby R G 1976 *Handbook of Thick Film Technology* (Isle of Man: Electrochemical Publications) p 50
[22] Bourcet J C and Fong F K 1974 *J. Chem. Phys.* **60** 34
[23] Riwotzki K, Meyssamy H, Kornowski A and Haase M 2000 *J. Phys. Chem.* B **104** 2824